Engineered Colorectal Cancer Tissue Recapitulates Key Attributes of a Patient-derived Xenograft Tumor Line

Iman Hassani[1], Benjamin Anbiah[1], Peyton Kuhlers[2], Nicole L. Habbit[1], Bulbul Ahmed[2], Martin J. Heslin[3], James A. Mobley[4, 5], Michael W. Greene[2,*], Elizabeth A. Lipke[1,*]

[1]Department of Chemical Engineering, Auburn University, Auburn, AL 36849, USA
[2]Department of Nutrition, Dietetics, and Hospitality Management, Auburn University, Auburn, AL 36849, USA
[3]Mitchell Cancer Institute, University of South Alabama, Mobile, AL 36604, USA.
[4]Department of Anesthesiology and Perioperative Medicine, School of Medicine, University of Alabama at Birmingham, Birmingham, AL 35205-3703, USA
[5]Division of Molecular and Translational Biomedicine, School of Medicine, University of Alabama at Birmingham, Birmingham, AL 35205-3703, USA
*Co-corresponding authors

Supplementary Figures, Data and Methods

The supplementary data for this article include the in-depth characterization of *in vitro* 3D engineered CRC-PDX (3D-eCRC-PDX) and the 2D-CRC-PDX cell culture characterization for comparison with 3D-eCRC-PDX tissues and the originating CRC-PDX tumors. **Supplementary Figure 1** shows a schematic of excision of CRC-PDX tumor pieces for mechanical stiffness measurement. **Supplementary Figure 2** demonstrates the viability of cells in 2D-CRC-PDX cell cultures and 3D-eCRC-PDX tissues. **Supplementary Figure 3** and **4** show temporal changes in cell numbers for 2D-CRC-PDX cultures and 3D-eCRC-PDX tissues, respectively. **Supplementary Figures 5-8** provide flow cytometry data examining temporal changes in the multiple PDX CRC-derived cell subpopulations for the CRC-PDX tumors, 3D-eCRC-PDX tissues, and 2D-CRC-PDX cultures. **Supplementary Figures 9** and **10** present confocal microscopy images of the labeled cells in the 3D-eCRC-PDX tissues and 2D-CRC-PDX cultures, respectively. **Supplementary Figures 11** and **12** provide the size and shape and machinal stiffness data for acellular poly(ethylene glycol)-fibrinogen (PEG-Fb) hydrogels. **Supplementary Figures 13-15** present the proteomics data. **Supplementary Figures 16-18** provide comparison data

obtained through analysis of the RNA seq results. Full descriptions of each figure are provided in the relevant figure legend.

All supporting flow cytometry data are provided following the supplementary figures. RNA seq data (GSE151069) for the CRC-PDX tumors and 3D-eCRC-PDX tissues are available from the NCBI Gene Expression Omnibus database (www.ncbi.nlm.nih.gov/geo). Proteomics data for the CRC-PDX tumors and 3D-eCRC-PDX tissues will be uploaded to the PRIDE - Proteomics Identification Database - EMBL-EBI upon acceptance of the manuscript.

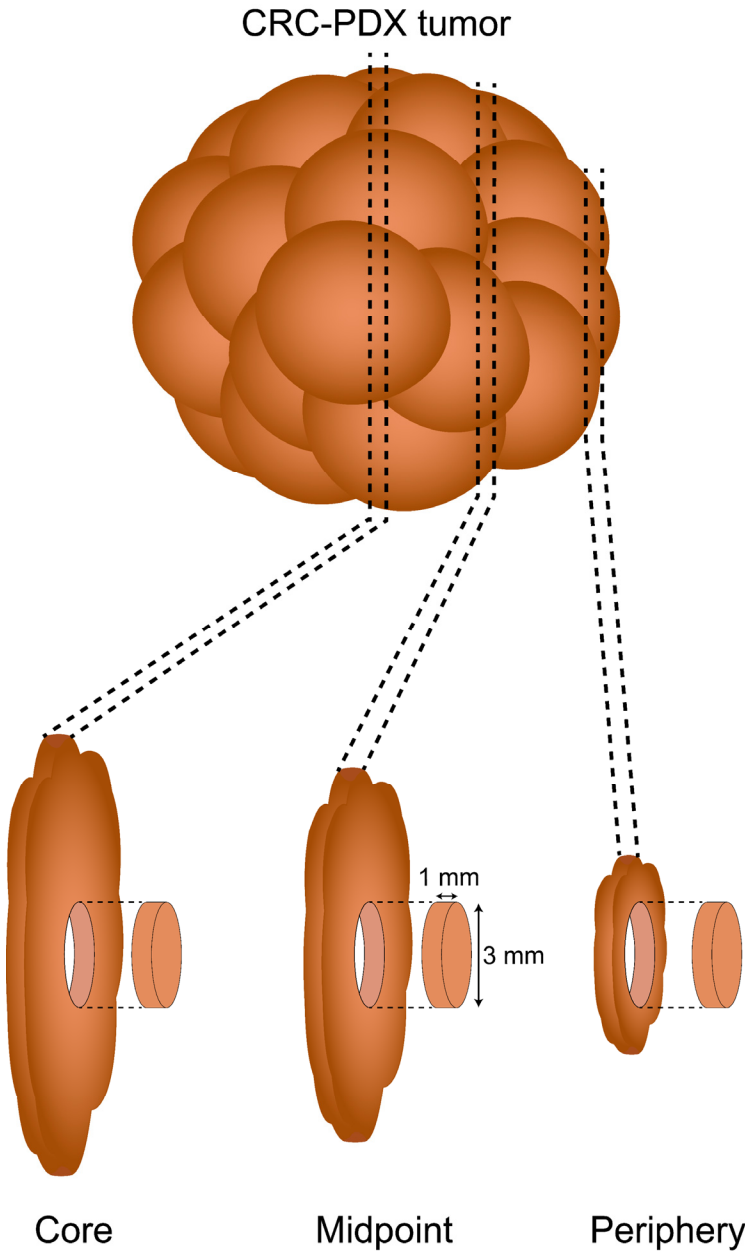

Supplementary Figure 1. Excision of CRC-PDX tumor pieces for mechanical stiffness measurement. The geometric core, midpoint, and periphery of CRC-PDX tumors were cut into disk-shaped slices using a sterile scalpel (Bard-Parker®). Subsequently, pieces with a diameter of approximately 3 mm and a thickness of approximately 1 mm (thus resembling the 3D-eCRC-PDX tissue geometry) were excised using a surgical punch (Sklar) for parallel compression testing.

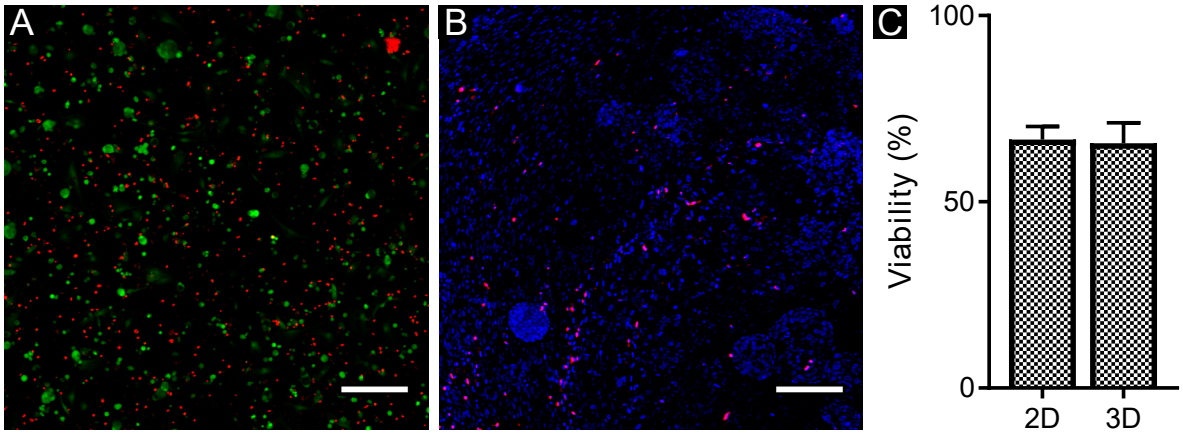

Supplementary Figure 2. Live/Dead assay quantification of cell viability. (A) Representative confocal microscopy images of live (green) and dead (red) cells in 2D-CRC-PDX cultures on Day 1 (Scale bar=200 µm). (B) Representative confocal microscopy images of cell nuclei (blue) counterstained with Hoechst 33342 and dead cells (red) within the 3D-eCRC-PDX tissues employed for cell viability quantification purposes (Scale bar=200 µm). (C) Approximately, 67 ± 4 percent of the 2D-CRC-PDX cells and 66 ± 6 percent of the cells within the 3D-eCRC-PDX tissues were viable on Day 1; there was no significant difference between conditions. Bars are mean ± SD ($p \leq 0.05$, n = 3 tissues or 2D-CRC-PDX cultures).

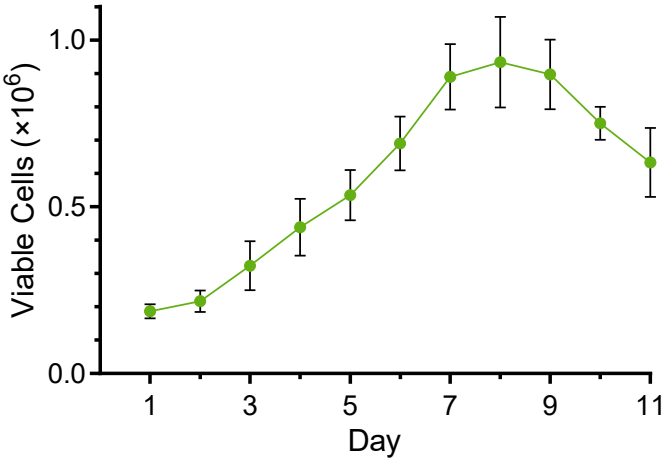

Supplementary Figure 3. CRC-PDX cell growth rate in 2D-CRC-PDX cultures without cell passaging. The total number of viable CRC-PDX cells, cultured in T25 flasks, increased from Day 1 to Day 8, at which point confluency was reached. A decrease in cell number was observed thereafter. Therefore, the 2D-CRC-PDX cells were passaged every 7 days for experiments comparing them to the 3D-eCRC-PDX tissues. Data are mean ± SD (n= 3 separate batches of cell cultures).

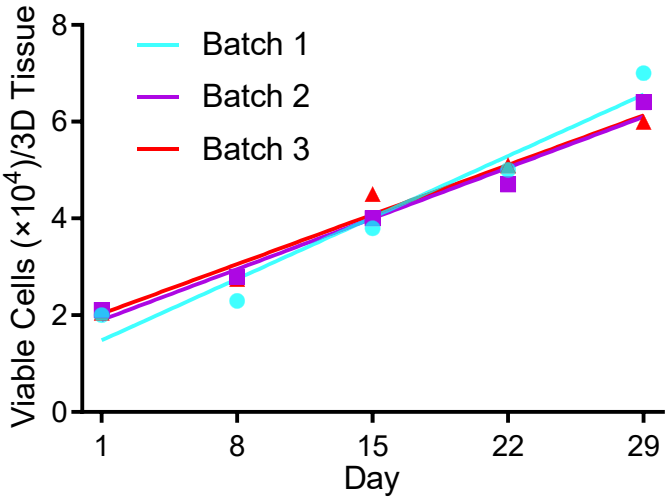

Supplementary Figure 4. Viable CRC-PDX cell numbers within the 3D-eCRC-PDX tissues. Following 3D-eCRC-PDX tissue dissociation and trypan blue staining, the viable cells were counted using a hemocytometer. The numbers of viable cells within the 3D-eCRC-PDX tissues increased from Day 1 to Day 29 for all 3 batches of cell culture. No significant difference was observed between the rates of increase (slopes) based on linear regression analysis ($p \leq 0.05$, n = 3 separately prepared batches).

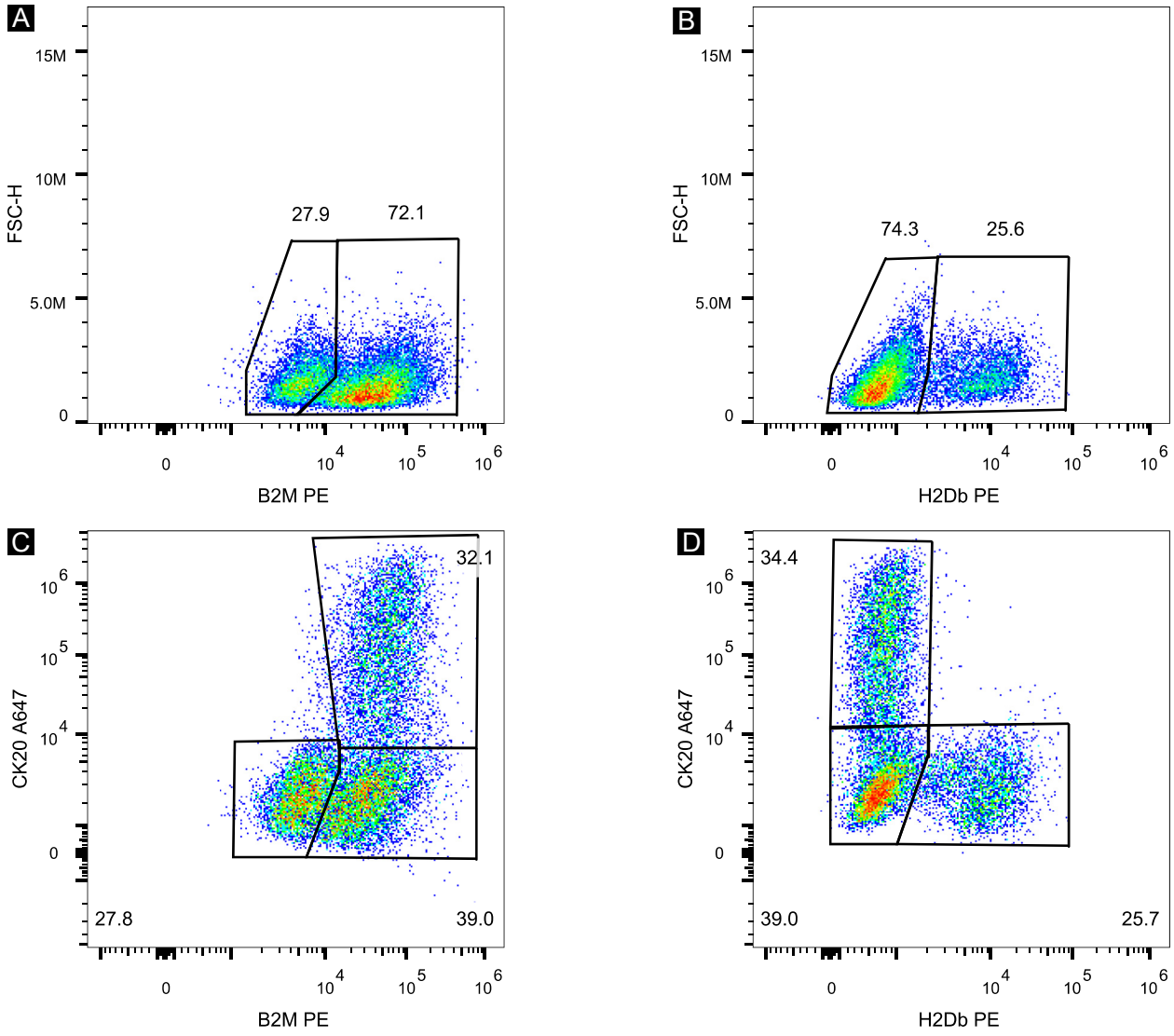

Supplementary Figure 5. Examination of human (B2M$^+$), mouse (H2Db$^+$), and CK20$^+$ cell subpopulations. One sample containing CRC-PDX cells was divided equally into two samples and the cells were labeled with β-2 microglobulin (B2M) and cytokeratin 20 (CK20) or H2Db and CK20. The percentage of (A) B2M$^-$ cells in sample 1 was approximately equal to that of (B) H2Db$^+$ cells in sample 2. Furthermore, all CK20$^+$ cells were also positive for (C) B2M and negative for (D) H2Db.

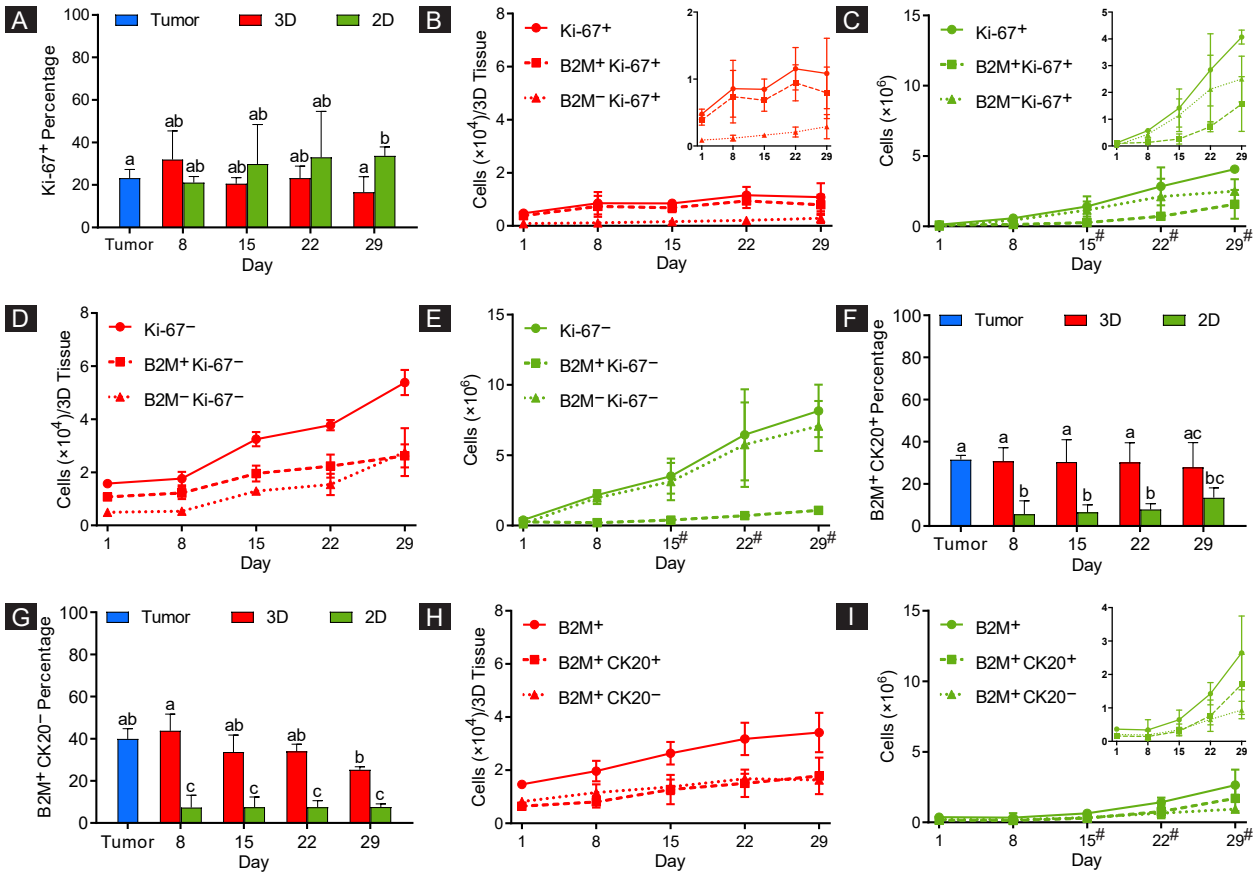

Supplementary Figure 6. Quantification of CRC PDX cell subpopulations through flow cytometry. (A) The total percentages of Ki-67$^+$ cells (B2M$^+$ and B2M$^-$) in the 3D-eCRC-PDX tissues and 2D-CRC-PDX cultures were similar to that in the CRC-PDX tumors, except for 2D-CRC-PDX cells on Day 29, which had a significantly higher percentage of proliferating cells (Ki-67$^+$) than the original CRC-PDX tumors. For 3D-eCRC-PDX tissues the rates of increase in (B) human proliferative (B2M$^+$ Ki67$^+$) and mouse proliferative (B2M$^-$ Ki-67$^+$) cell numbers were similar, maintaining a ratio equivalent to the original tumor. In sharp contrast, (C) for 2D-CRC-PDX cultures, mouse cells were the major contributor to the total proliferative cell number increase, whereas human proliferative cell number increased at significantly lower rates (0.53±0.07 fold). Similarly, the (D) human non-proliferative (B2M$^+$ Ki-67$^-$) and mouse non-proliferative (B2M$^-$ Ki-67$^-$) cell numbers increased with similar rates in the 3D-eCRC-PDX tissues, whereas (E) in 2D-CRC-PDX cultures, human non-proliferative cell number increased at significantly lower rates compared to mouse non-proliferative cells (0.12±0.01 fold). (F, G) The 3D-eCRC-PDX tissues maintained B2M$^+$ CK20$^+$ and B2M$^+$ CK20$^-$ cell subpopulations over time, whereas in 2D-CRC-PDX cultures, these cell subpopulations decreased significantly after 8 days of culture and remained unchanged thereafter. (H, I) B2M$^+$ CK20$^+$ and B2M$^+$ CK20$^-$ cell subpopulations increased ratiometrically in the 3D-eCRC-PDX tissues whereas the rates of increase in 2D-CRC-PDX cultures were lower during initial days of culture compared to later time points. Data are mean ± SD. Means that do not share a letter are significantly different ($p \leq 0.05$, n=3 separate batches of cell culture). # indicates that the 2D-CRC-PDX cells were passaged at the previous time point.

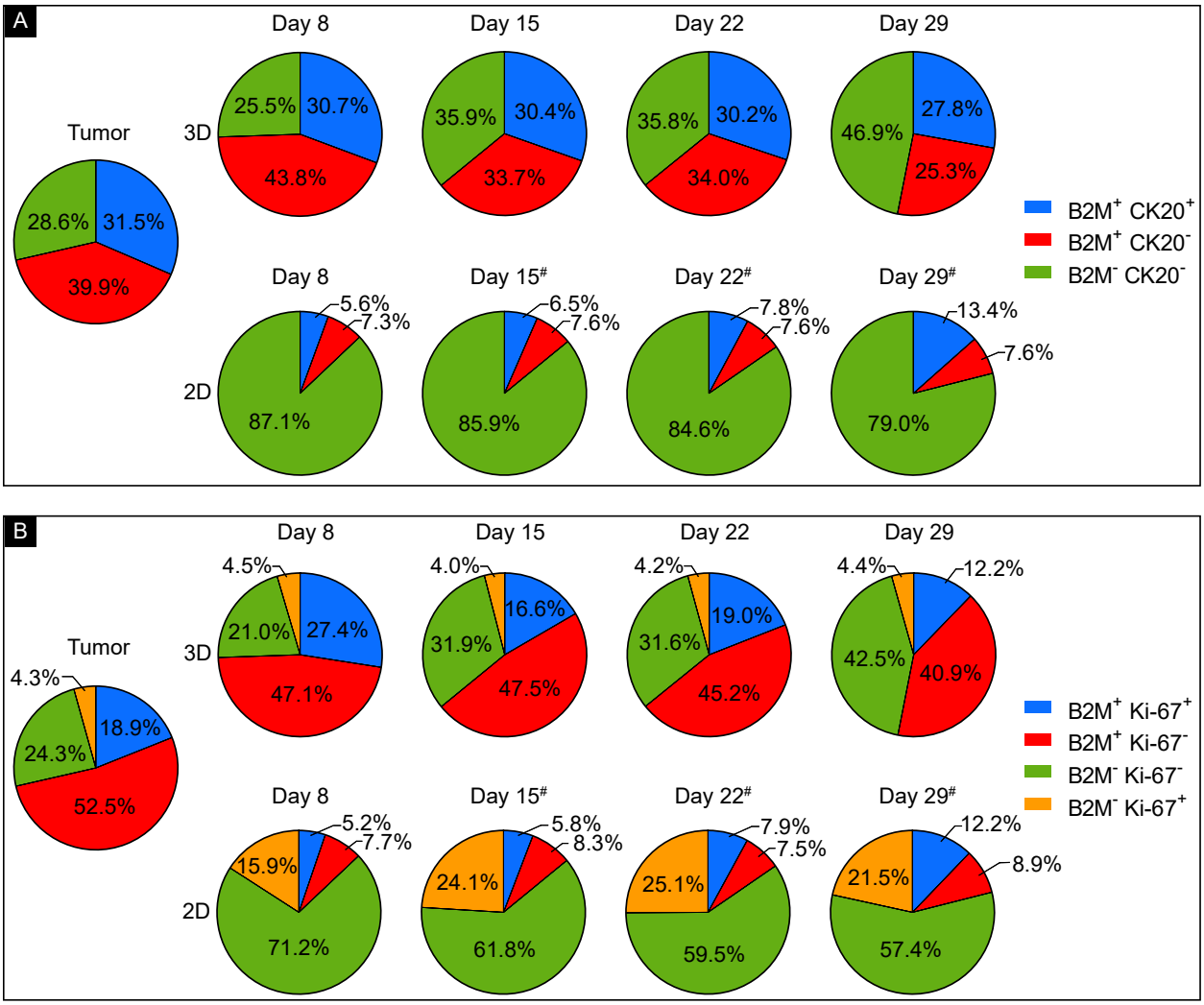

Supplementary Figure 7. Cell subpopulations within the CRC-PDX tumors, 3D-eCRC-PDX tissues, and 2D-CRC-PDX cultures. Flow cytometry analysis using B2M, CK20, and Ki-67 markers showed that different CRC-PDX cell subpopulations within 3D-eCRC-PDX tissues were similar to the CRC-PDX tumors over time, whereas the 2D-CRC-PDX cell subpopulations displayed a significant deviation from the CRC-PDX tumors. # indicates that the 2D-CRC-PDX cells were passaged at the previous time point.

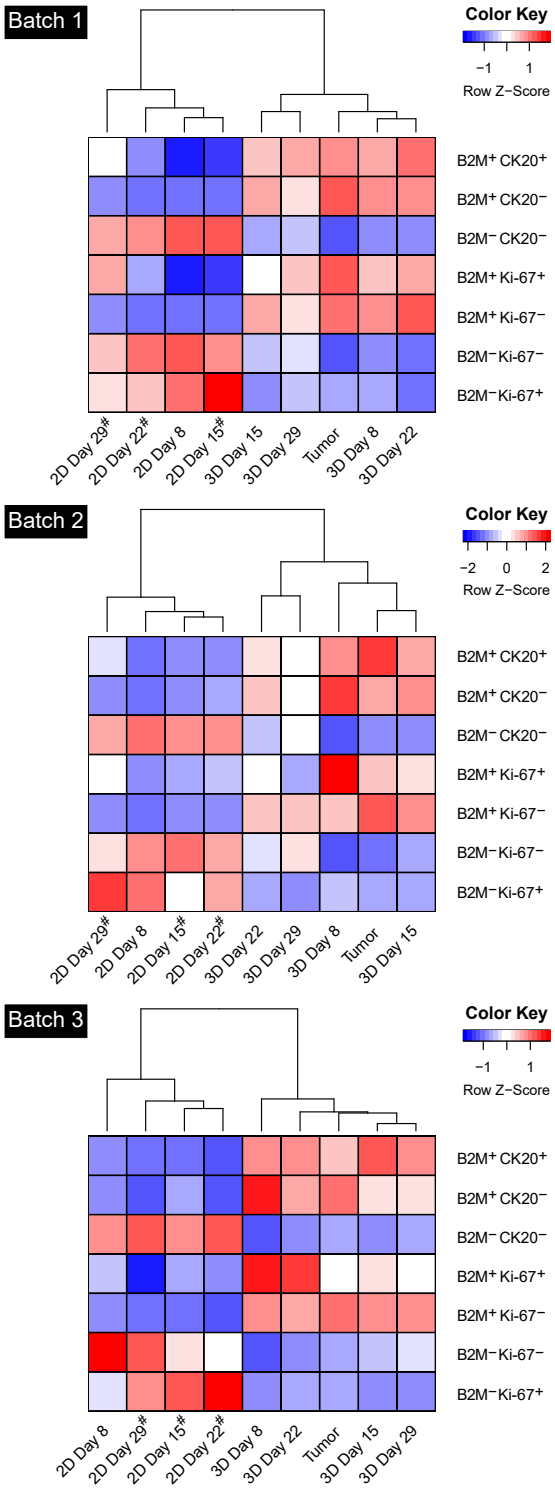

Supplementary Figure 8. Cluster analysis of the cell subpopulations obtained from flow cytometry results. For three separate batches of cell culture, the 3D-eCRC-PDX tissues clustered with the CRC-PDX tumors whereas the 2D-CRC-PDX cells clustered separately from both the 3D-eCRC-PDX tissues and CRC-PDX tumors. # indicates that the 2D-CRC-PDX cells were passaged at the previous time point.

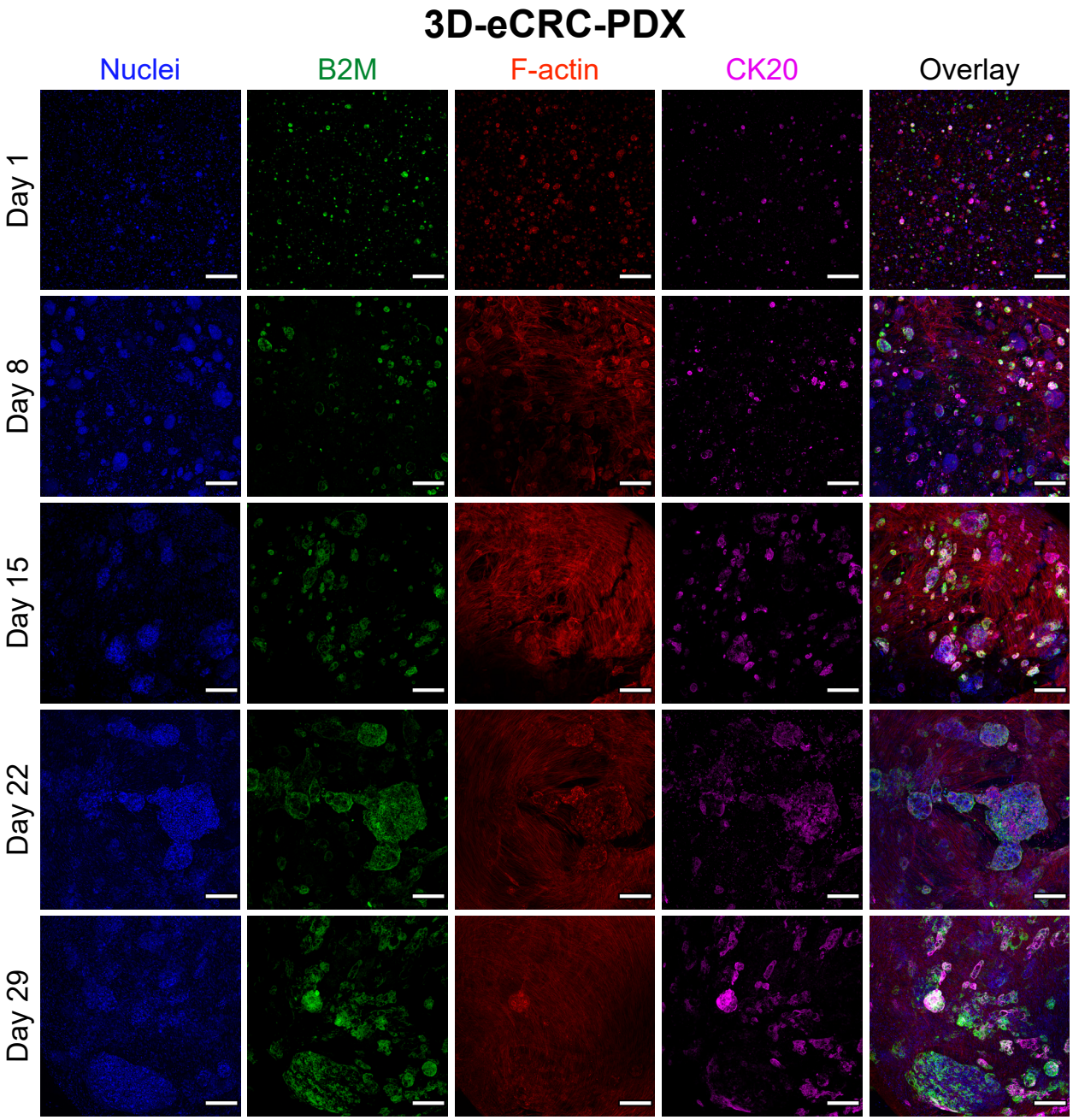

Supplementary Figure 9. Staining of cells within the 3D-eCRC-PDX tissues. Cells within the 3D-eCRC-PDX tissues were labeled with Hoechst 33342 (blue), B2M (green), phalloidin (red), and CK20 (magenta). Human ($B2M^+$) and $CK20^+$ formed colonies whereas mouse ($B2M^-$) cells exhibited elongation. The size of cell colonies and the density of elongated cells increased from Day 1 to Day 29 (scale bar = 200 µm).

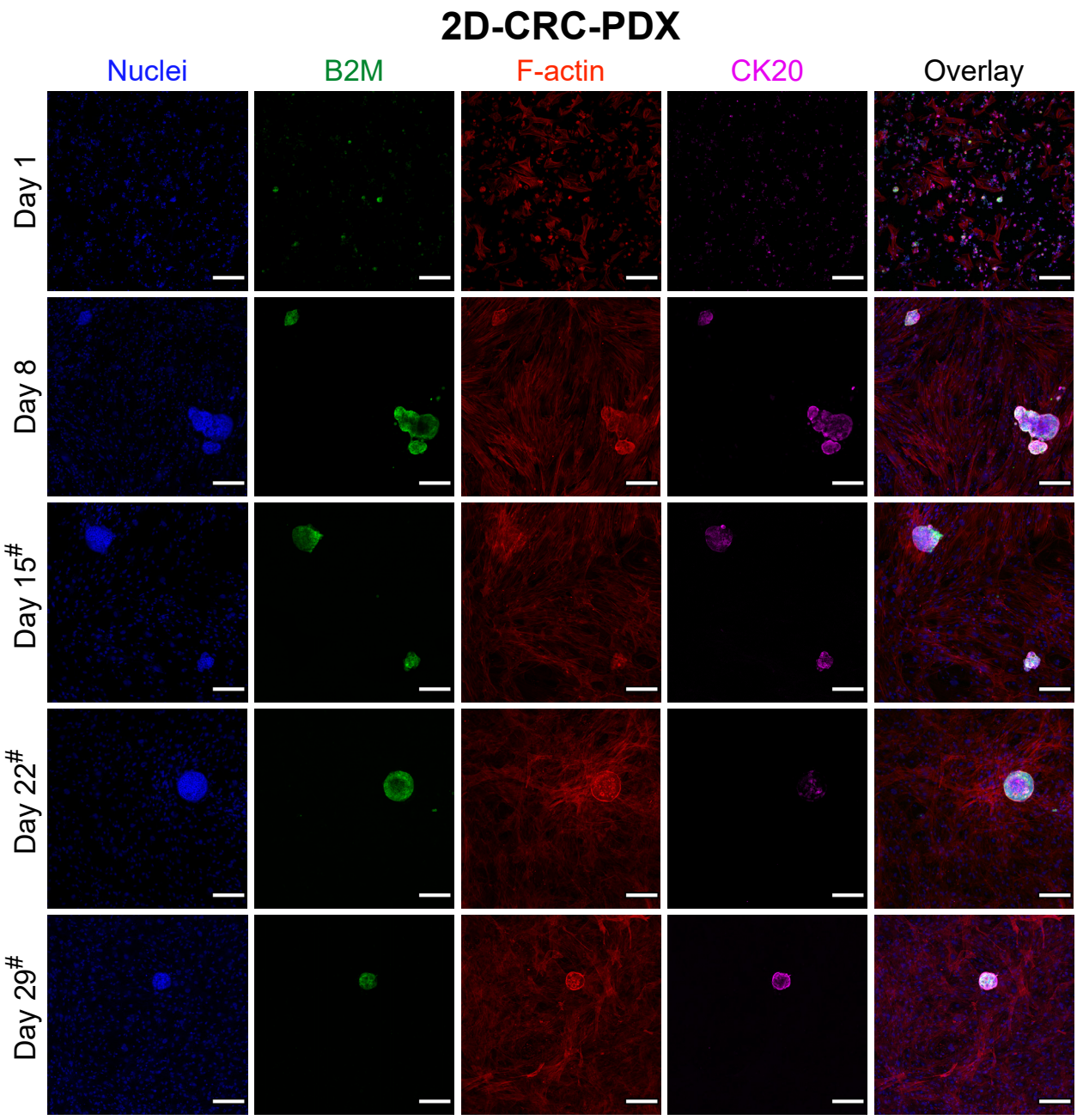

Supplementary Figure 10. Staining of 2D-CRC-PDX cells. The 2D-CRC-PDX cells were labeled with Hoechst 33342 (blue), B2M (green), phalloidin (red), and CK20 (magenta). Human ($B2M^+$) and $CK20^+$ cells formed colonies whereas mouse ($B2M^-$) cells exhibited elongation (scale bar = 200 µm). # indicates that the 2D-CRC-PDX cells were passaged at the previous time point.

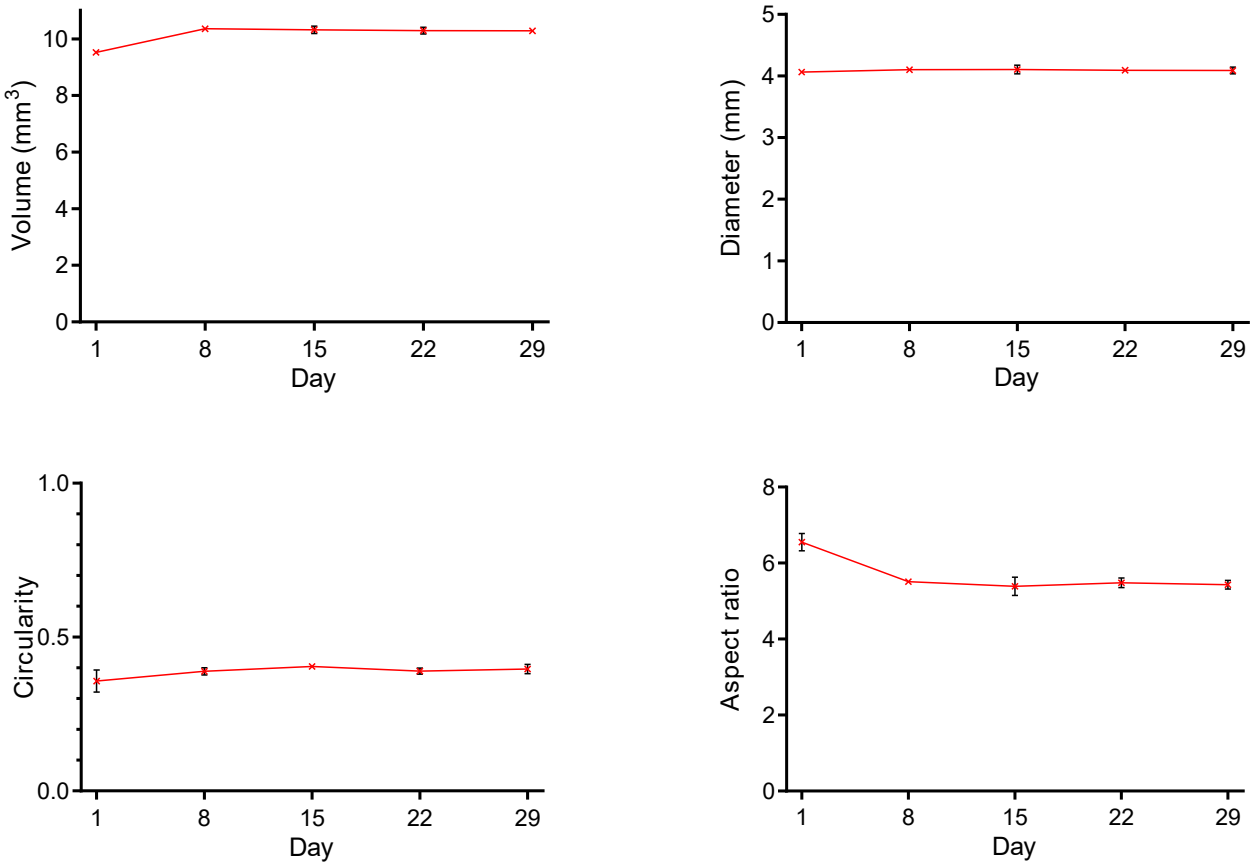

Supplementary Figure 11. Size and shape of acellular PEG-Fb hydrogels over time. The volume of acellular hydrogels increased slightly from Day 1 to Day 8 and remained constant thereafter. The diameter and circularity of the acellular hydrogels remained constant over time. The aspect ratio of the acellular hydrogels decreased from Day 1 to Day 8 and remained constant thereafter. Data are mean ± SD (n=3 acellular hydrogels).

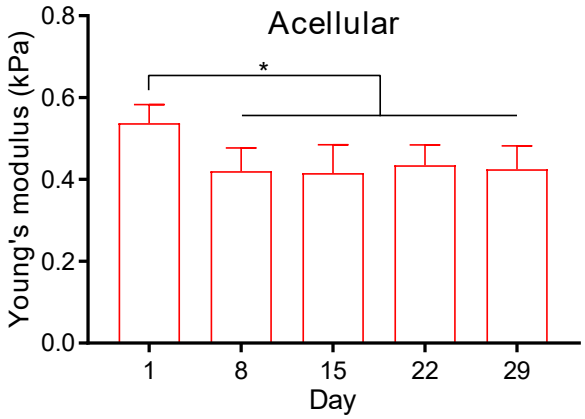

Supplementary Figure 12. Mechanical stiffness of the acellular hydrogels. The stiffness of acellular hydrogels was found to decrease from Day 1 to Day 8 and remained constant thereafter. Data are mean ± SD ($p \leq 0.05$, n=3 acellular hydrogels).

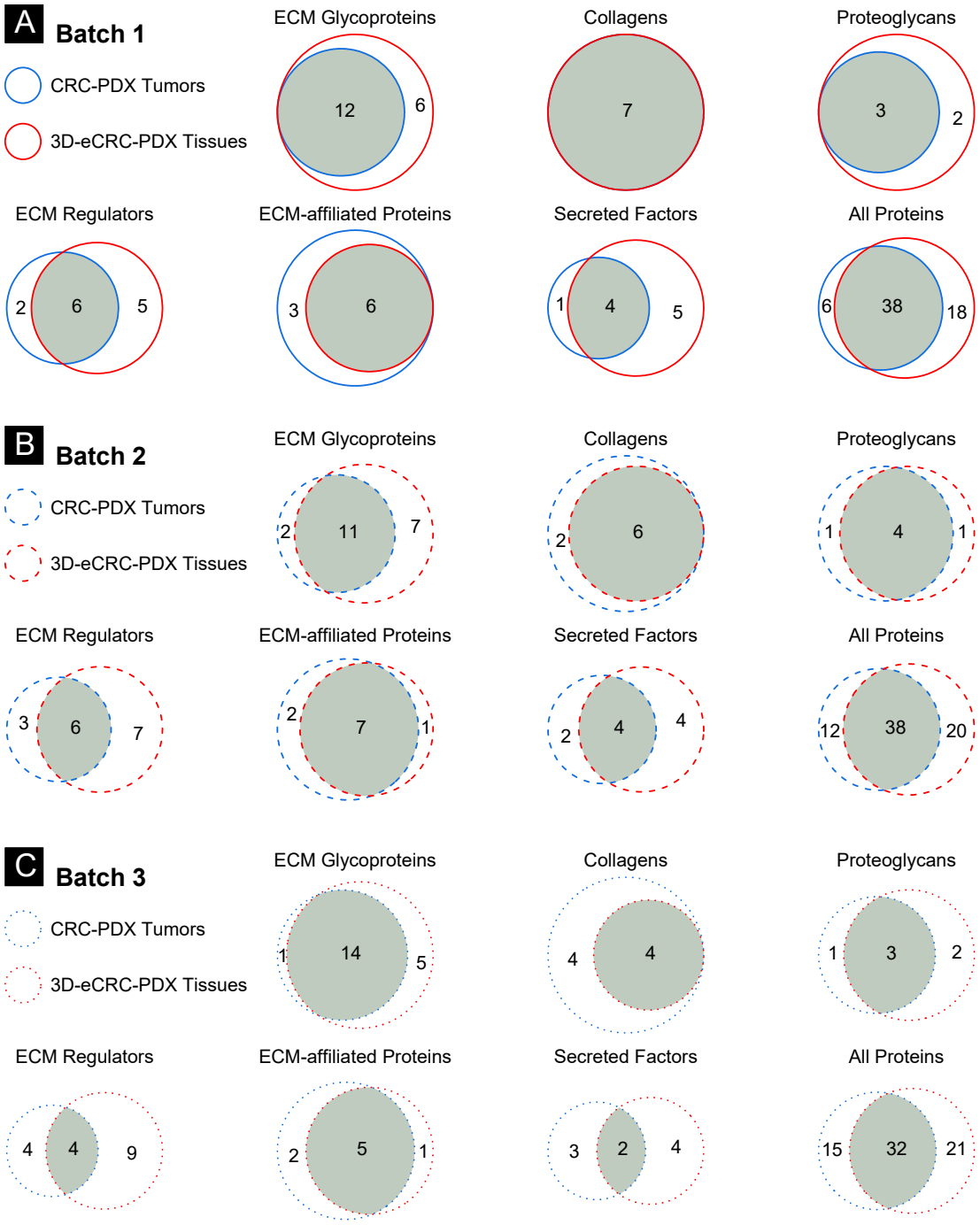

Supplementary Figure 13. Comparison of identified extracellular matrix (ECM) proteins in CRC-PDX tumors and 3D-eCRC-PDX tissues. The numbers of shared, CRC-PDX tumor-specific and 3D-eCRC-PDX tissue-specific proteins for Batch 1, 2, and 3 are shown. (A) In batch 1, approximately 61% of identified ECM proteins were observed in both CRC-PDX tumors and 3D-eCRC-PDX tissues. Similarly, (B) in batch 2 approximately 54% of identified ECM proteins were observed in both the CRC-PDX tumor and the 3D-eCRC-PDX tissues, while (C) in batch 3, approximately 47% of proteins were found in both CRC-PDX tumors and 3D-eCRC-PDX tissues.

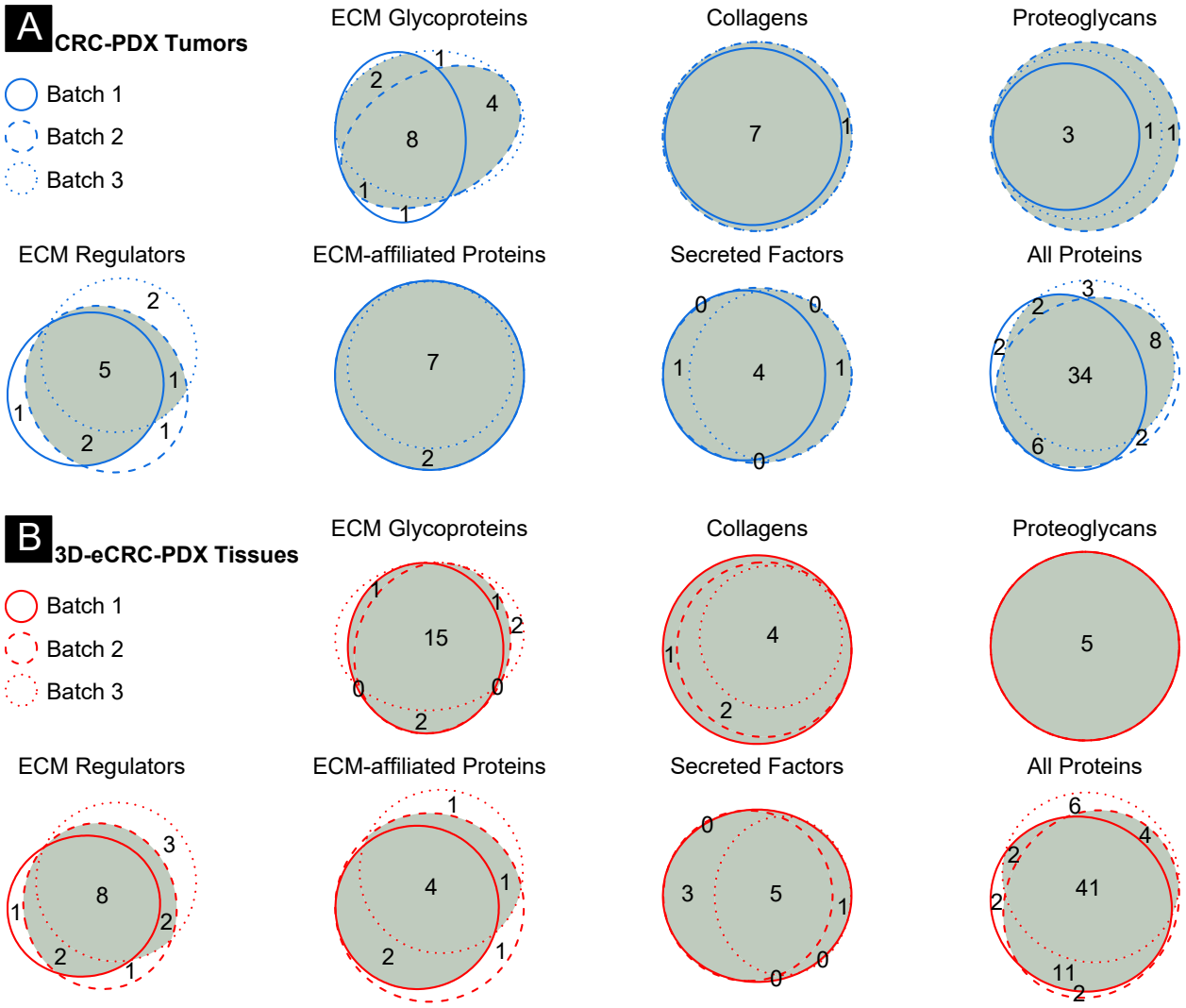

Supplementary Figure 14. Protein batch-to-batch consistency between CRC-PDX tumors or 3D-eCRC-PDX tissues. (A) Approximately 60% of ECM proteins within CRC-PDX tumors were the same for all three batches, 28% of the ECM proteins were present in at least two batches, and 12% of the ECM proteins were specific to each batch. (B) For 3D-eCRC-PDX tissues, 60% of ECM proteins were found to be the same for all batches, 25% were present in at least two batches, and 15% were batch-specific.

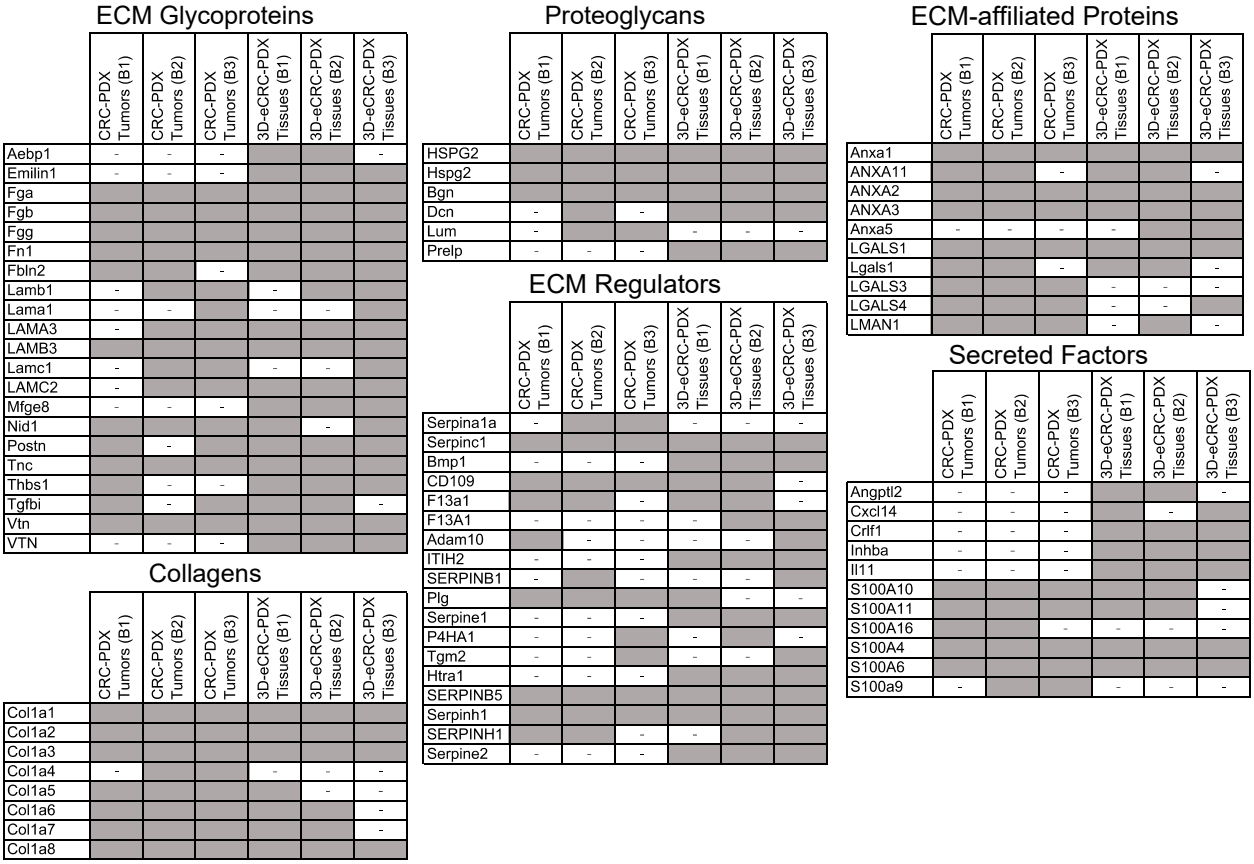

Supplementary Figure 15. Comparison between the identified ECM proteins in CRC-PDX tumors and 3D-eCRC-PDX tissues from Batch 1 (B1), Batch 2 (B2), and Batch 3 (B3). The ECM proteins identified in only one out of six samples (CRC-PDX tumors and 3D-eCRC-PDX tissues) were removed from the analysis. A protein was indicated as present (gray cell) when the protein was detected in at least two out three samples and as absent (cell with a minus sign) when the protein was detected in only one sample or was not detected at all. Proteins presented in uppercase and lowercase letters are from human and mouse databases, respectively.

3D-eCRC-PDX Tissues

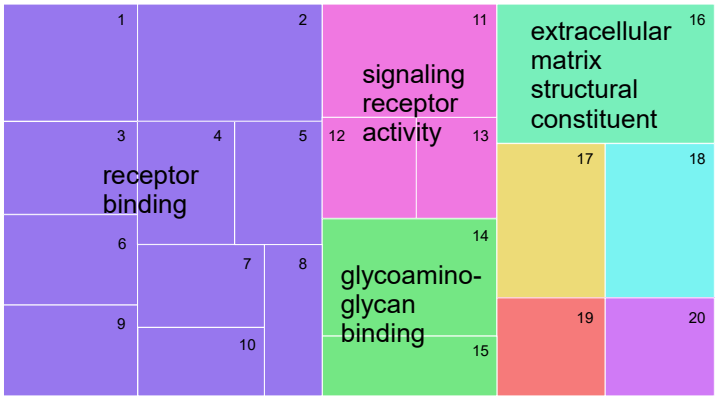

	term_ID	description	log10 FDR pvalue
1	GO:0005102	receptor binding	-8.9318
2	GO:0019955	cytokine binding	-5.3595
3	GO:0008009	chemokine activity	-4.757
4	GO:0048018	receptor agonist activity	-4.5544
5	GO:0005125	cytokine activity	-4.1325
6	GO:0019838	growth factor binding	-4.6635
7	GO:0005518	collagen binding	-3.9788
8	GO:0019956	chemokine binding	-3.3098
9	GO:0038085	VEGF binding	-4.6364
10	GO:0001968	fibronectin binding	-3.3279
11	GO:0038023	signaling receptor activity	-7.5719
12	GO:0015026	coreceptor activity	-3.6162
13	GO:0005044	scavenger receptor activity	-3.1325
14	GO:0005539	glycosaminoglycan binding	-7.8477
15	GO:0008201	heparin binding	-3.9957
16	GO:0005201	ECM structural constituent	-11.385
17	GO:0030246	carbohydrate binding	-6.3788
18	GO:0060089	molecular transducer activity	-6.2716
19	GO:0005509	calcium ion binding	-4.0278
20	GO:0030545	receptor regulator activity	-3.983

CRC-PDX Tumors

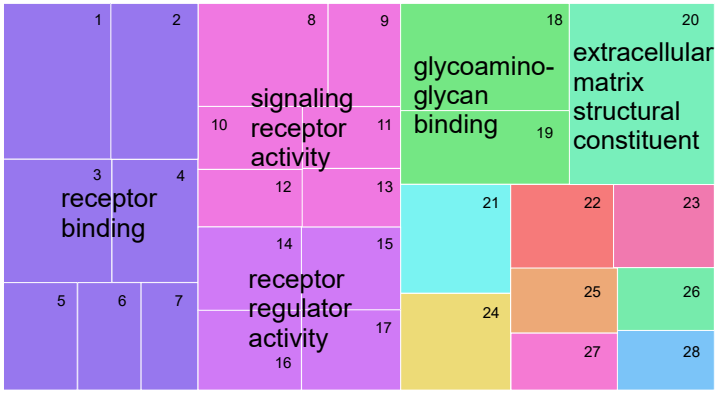

	term_ID	description	log10 FDR pvalue
1	GO:0005102	receptor binding	-9.1555
2	GO:0019838	growth factor binding	-7.4949
3	GO:0019955	cytokine binding	-7.3279
4	GO:0005518	collagen binding	-5.7986
5	GO:0038085	VEGF binding	-4.4023
6	GO:0043394	proteoglycan binding	-3.8097
7	GO:0019956	chemokine binding	-3.3468
8	GO:0038023	signaling receptor activity	-7.4112
9	GO:0038024	cargo receptor activity	-4.1415
10	GO:0004955	prostaglandin receptor activity	-3.585
11	GO:0005044	scavenger receptor activity	-3.3696
12	GO:0030545	receptor regulator activity	-4.5229
13	GO:0015026	coreceptor activity	-3.1979
14	GO:0048018	receptor agonist activity	-4.6861
15	GO:0030545	receptor regulator activity	-4.5229
16	GO:0005125	cytokine activity	-4.5969
17	GO:0042379	chemokine receptor binding	-4.4012
18	GO:0005539	glycosaminoglycan binding	-10.004
19	GO:0008201	heparin binding	-6.8041
20	GO:0005201	ECM structural constituent	-14.248
21	GO:0060089	molecular transducer activity	-6.5784
22	GO:0005509	calcium ion binding	-4.6882
23	GO:1901681	sulfur compound binding	-4.5017
24	GO:0030246	carbohydrate binding	-5.7905
25	GO:0050840	extracellular matrix binding	-3.8633
26	GO:0098772	molecular function regulator	-3.2874
27	GO:0005198	structural molecule activity	-3.3536
28	GO:0005515	protein binding	-3.1085

Supplementary Figure 16. Gene ontology analysis of molecular functions enriched in CRC-PDX tumor and 3D-eCRC-PDX tissue samples. Enriched gene molecular function ontologies between CRC-PDX tumor (n=3) and 3D-eCRC-PDX tissue samples (n=3) and tumor-adjacent (normal) colon tissue (n=41) from The Cancer Genome Atlas Colon Adenocarcinoma (TCGA-COAD) determined using the Gorilla application were analyzed for redundancy using REVIGO [1]. The 'superclusters' of similar gene ontology (GO) terms are visualized with similar colors. The size of individual rectangles reflects false discovery rate (FDR) p-values: large rectangles represent low log10 FDR p values. Shown are GO term ID, description, and log10 FDR *p* value.

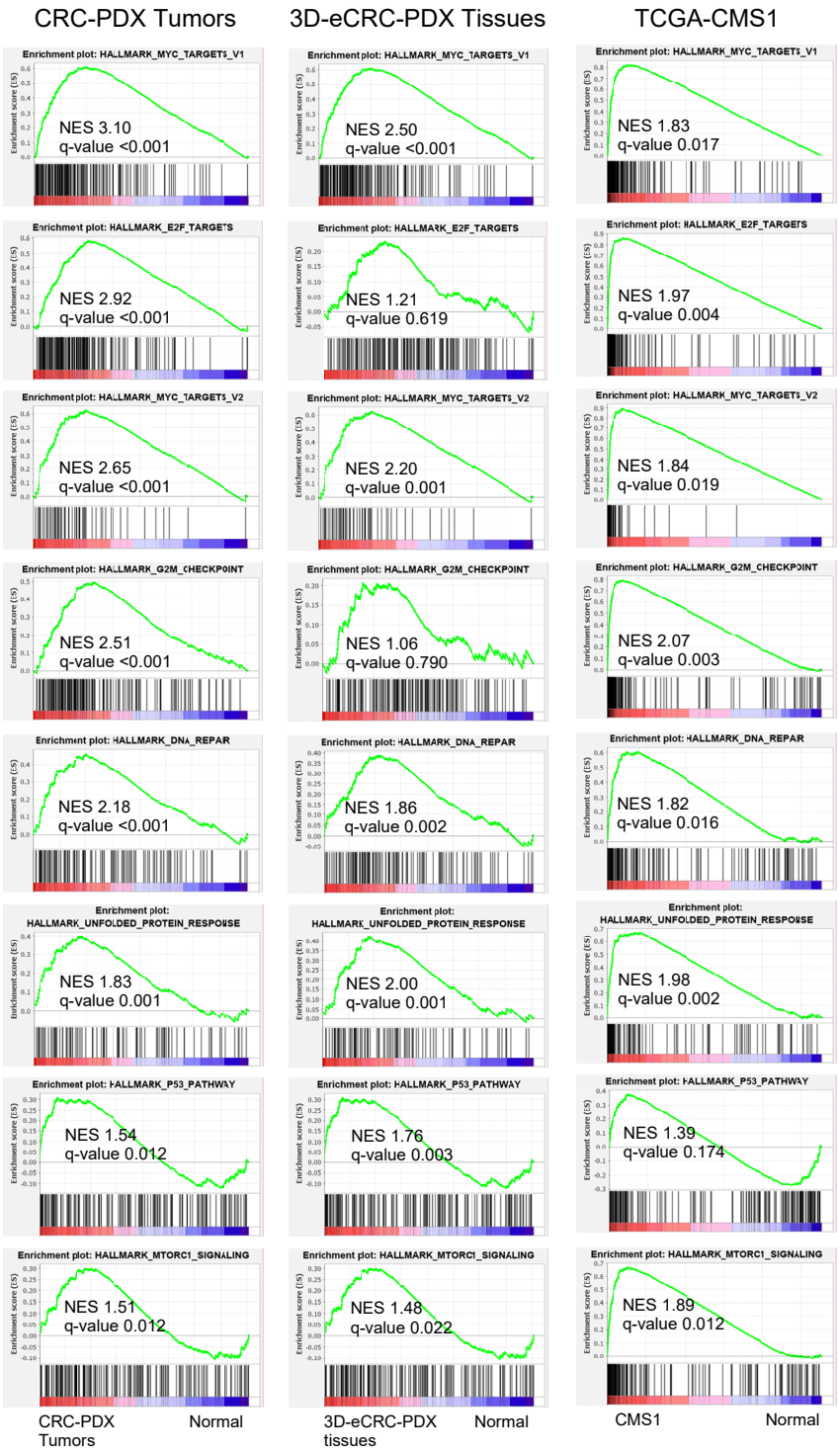

Supplementary Figure 17. Gene Set Enrichment Analysis (GSEA). The top 10 enriched gene set in the Molecular Signature Database (MSigDB) Hallmarks v7.0 gene sets in CRC-PDX tumor (n=3) (*upper left panel*), 3D-eCRC-PDX tissue (n=3) (*middle left panel*) and patient CRC tumor TCGA-COAD samples (n=84) (*lower left panel*) compared to tumor-adjacent (normal) colon tissue (n=41) from the TCGA-COAD. Enrichment plots with the normalized enrichment score (NES) and the FDR q-value are shown.

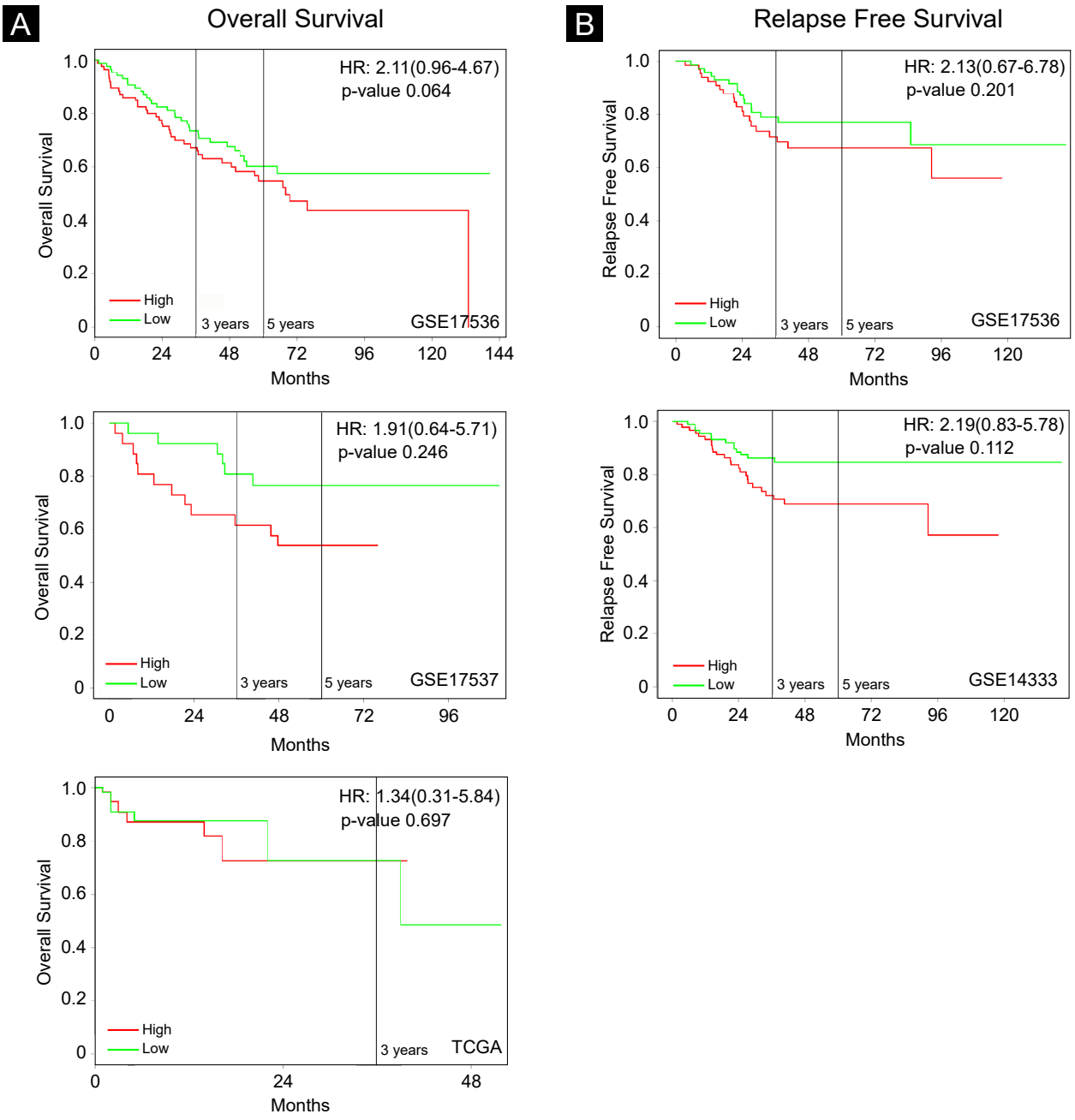

Supplementary Figure 18. Prognostic Kaplan–Meier survival analysis. Expression of the top 16 significantly upregulated genes between CRC-PDX tumors (n=3) and 3D-eCRC-PDX tissues (n=3) in the precomputed GEO dataset GSE17536 (n=174), GSE17537 (n=54), TCGA-COAD (n=121), GSE14333 (n=187) adjusted for age, stage, and gender covariates and bifurcated based on median expression was examined for overall survival (A) and relapse free survival (B). The hazard ratios, 95% confidence intervals, and p-values were shown.

Supplementary Table 1. Summary of the sequencing reads alignment to the reference genomes for the CRC-PDX

	Human		Mouse	
	3D†	CRC-PDX‡	3D†	CRC-PDX‡
All reads	180,572,171	189,200,637	180,572,171	189,200,637
All mapped reads	132,850,961	151,403,899	44,521,654	29,455,993
All mapped rate	73.6%	80.0%	24.7%	15.6%
Uniquely mapped reads	112,081,097	122,236,260	37,690,851	21,975,889
Uniquely mapped rate	62.1%	64.6%	20.9%	11.6%

†3D-eCRC-PDX tissues
‡CRC-PDX tumors

Supporting Flow Cytometry Data

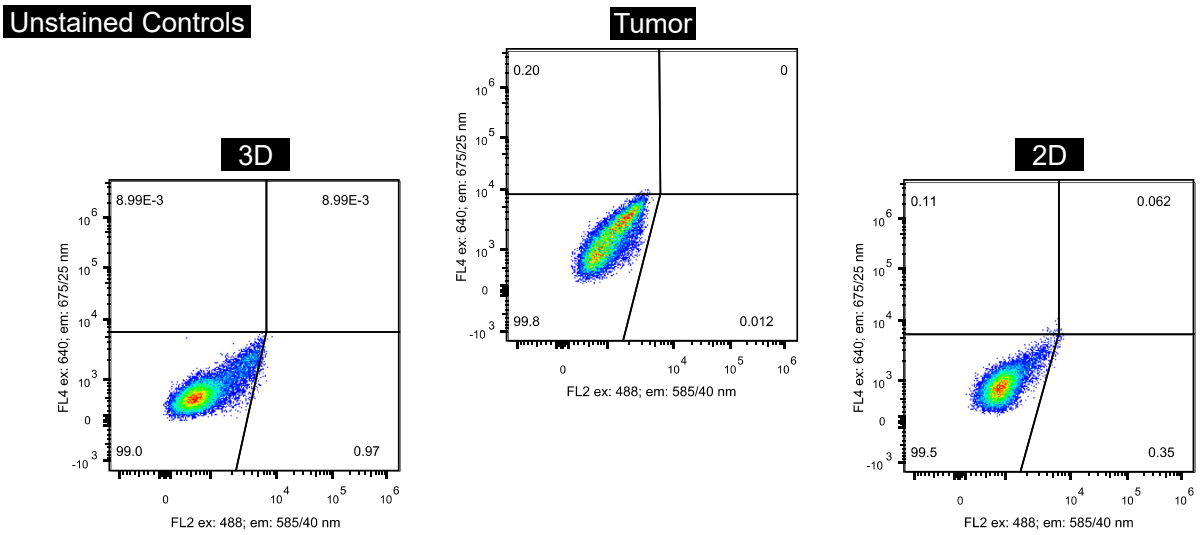

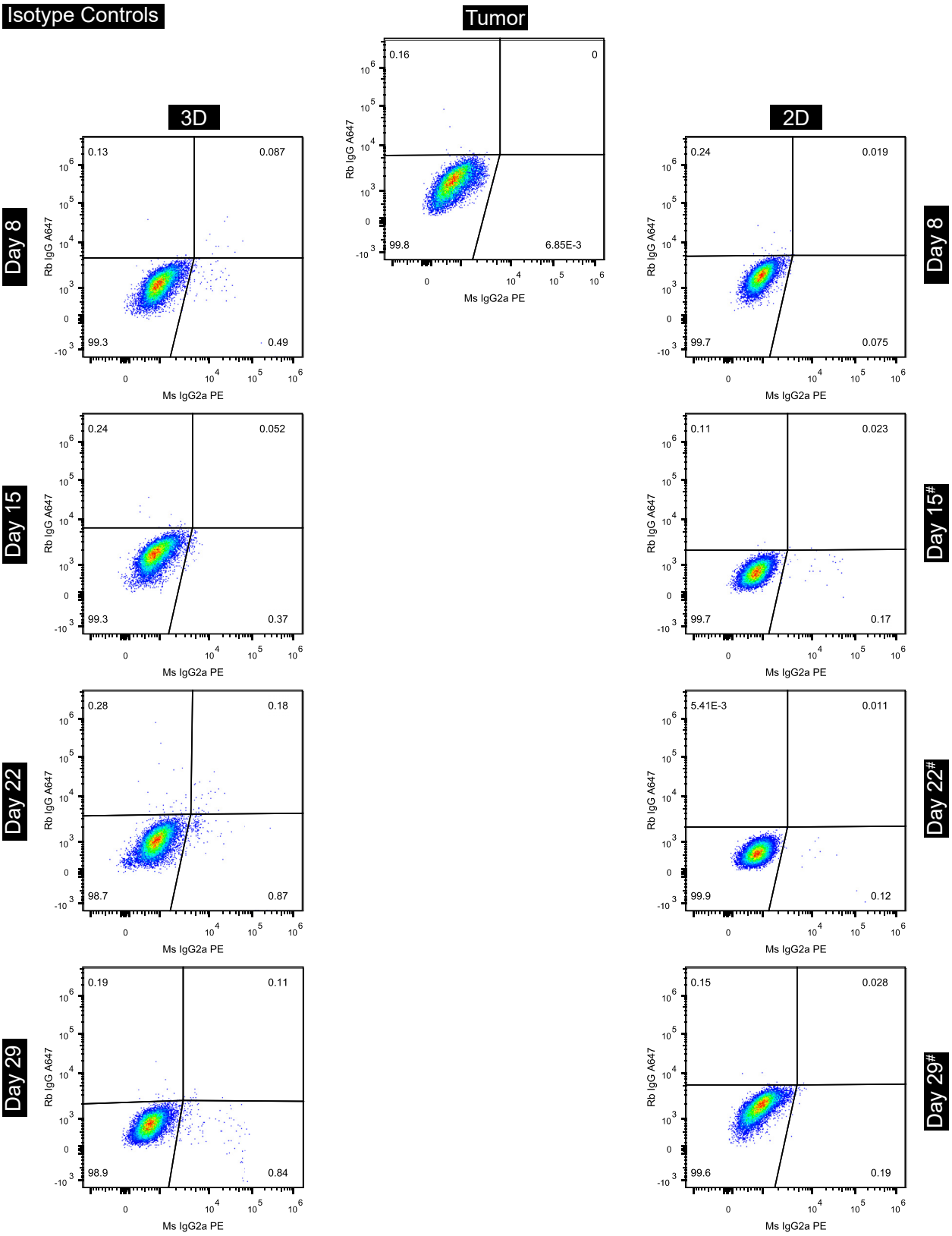
Isotype Controls
Tumor
3D
2D
Day 8
Day 15
Day 22
Day 29
Day 15#
Day 22#
Day 29#
Rb IgG A647
Ms IgG2a PE
0.16
0
99.8
6.85E-3
0.13
0.087
99.3
0.49
0.24
0.019
99.7
0.075
0.24
0.052
99.3
0.37
0.11
0.023
99.7
0.17
0.28
0.18
98.7
0.87
5.41E-3
0.011
99.9
0.12
0.19
0.11
98.9
0.84
0.15
0.028
99.6
0.19

Batch 1
B2M and CK20

Tumor

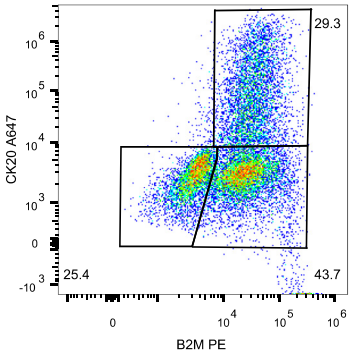

3D

2D

Day 8

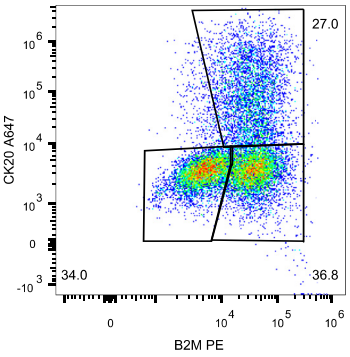

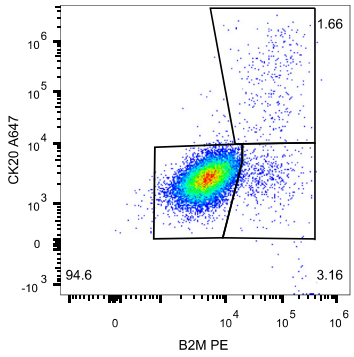

Day 8

Day 15

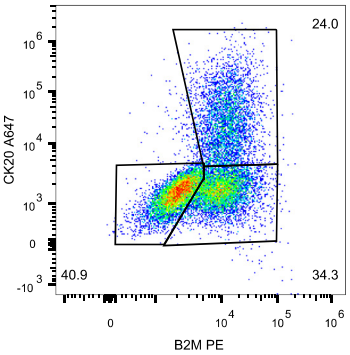

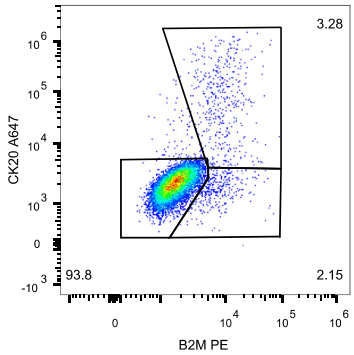

Day 15#

Day 22

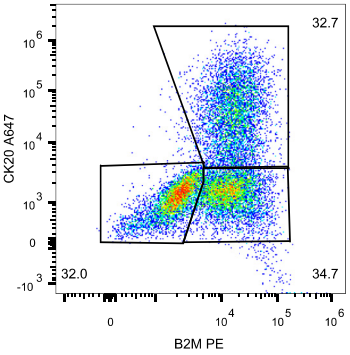

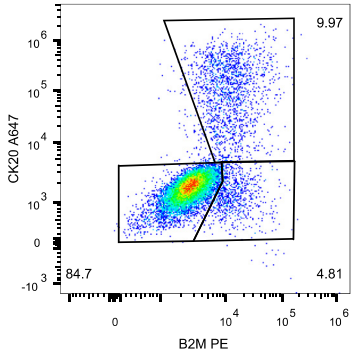

Day 22#

Day 29

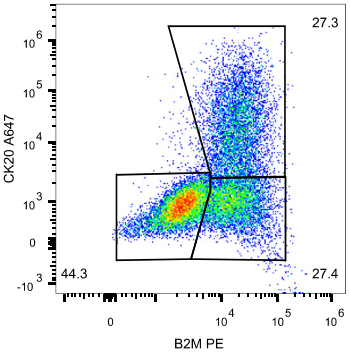

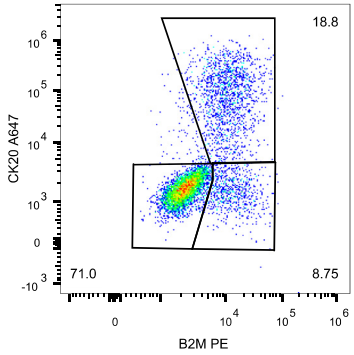

Day 29#

Batch 1
B2M and Ki-67

Tumor

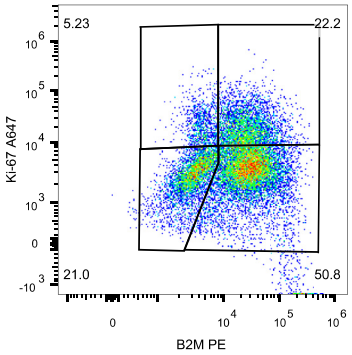

3D

2D

Day 8

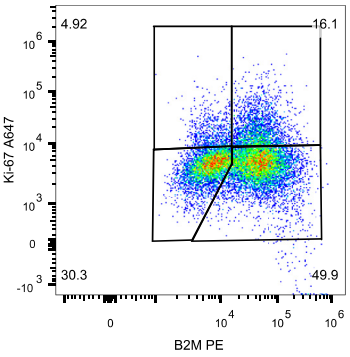

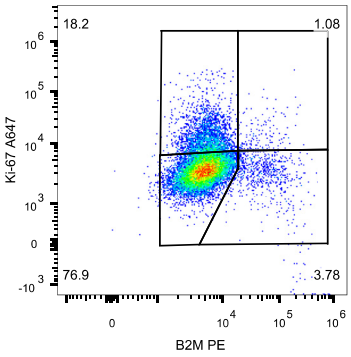

Day 8

Day 15

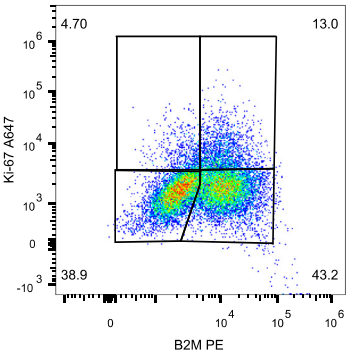

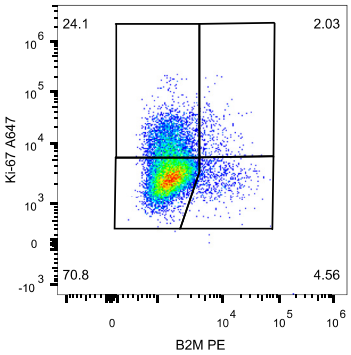

Day 15#

Day 22

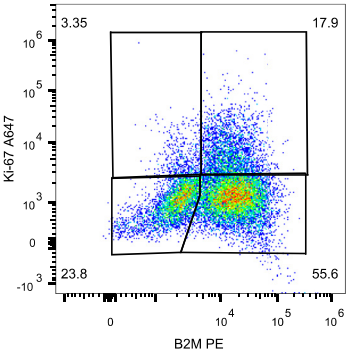

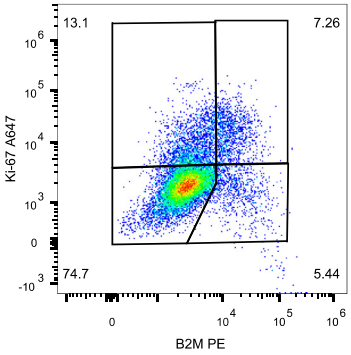

Day 22#

Day 29

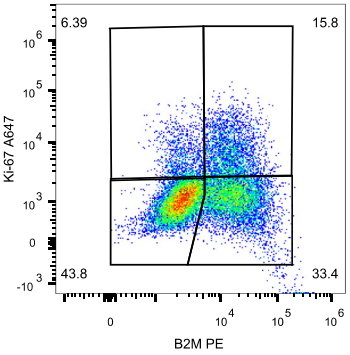

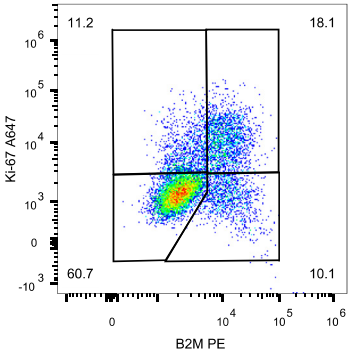

Day 29#

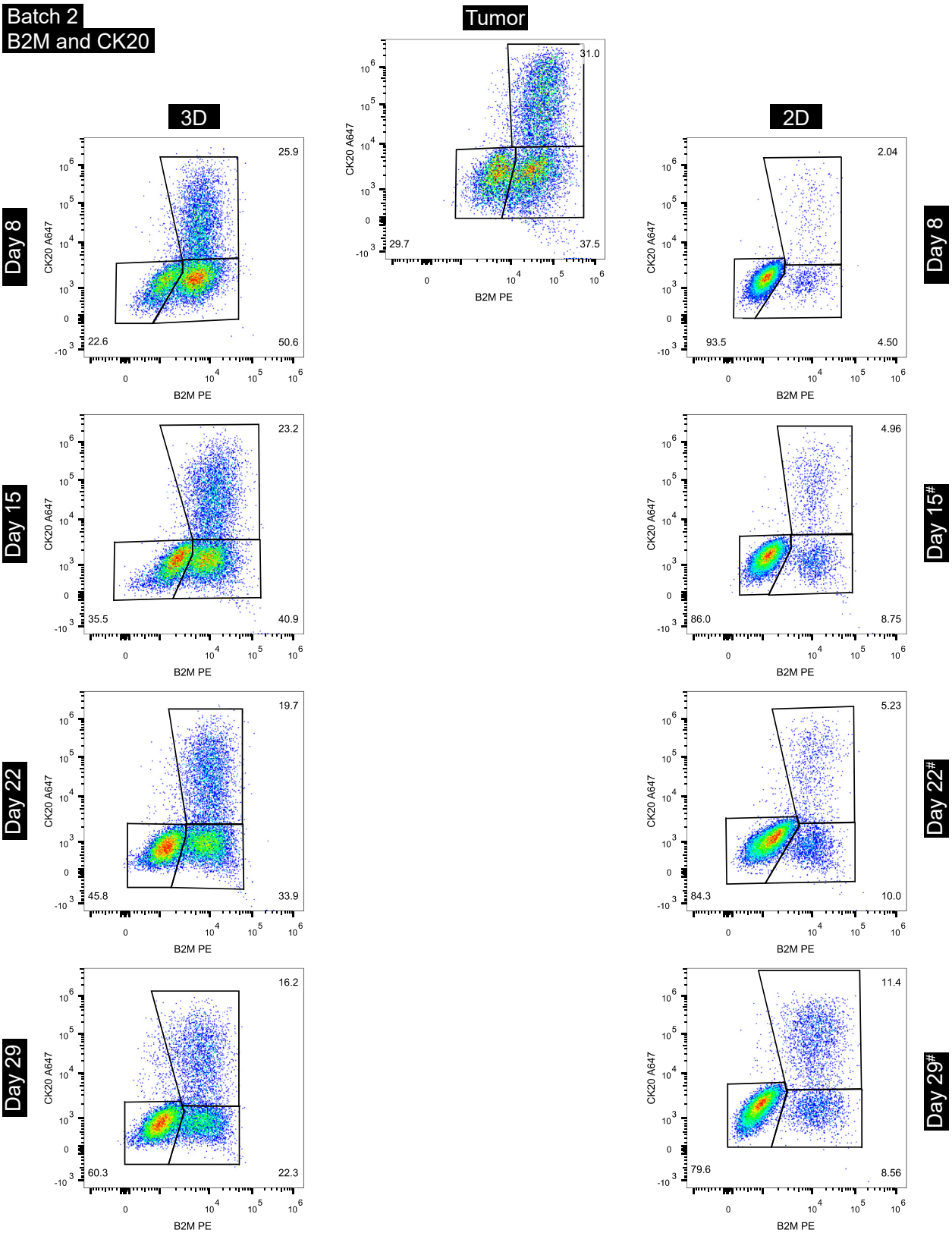
Batch 2
B2M and CK20
Tumor
3D
2D
Day 8
Day 15
Day 22
Day 29
Day 8
Day 15#
Day 22#
Day 29#
CK20 A647
B2M PE
31.0
29.7
37.5
25.9
22.6
50.6
2.04
93.5
4.50
23.2
35.5
40.9
4.96
86.0
8.75
19.7
45.8
33.9
5.23
84.3
10.0
16.2
60.3
22.3
11.4
79.6
8.56

Batch 2
B2M and Ki-67

Tumor

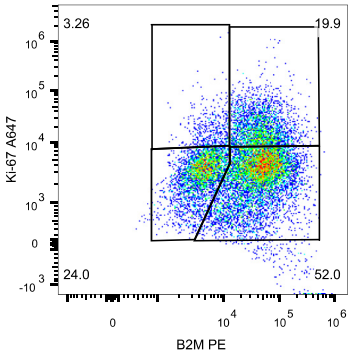

3D

2D

Day 8

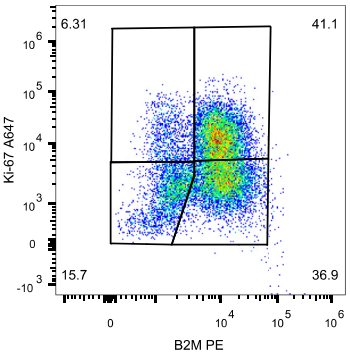

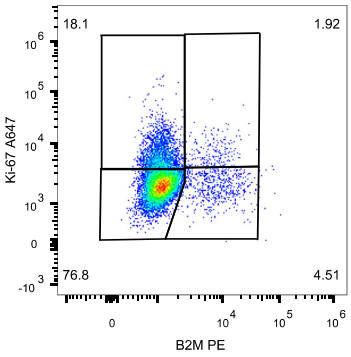

Day 8

Day 15

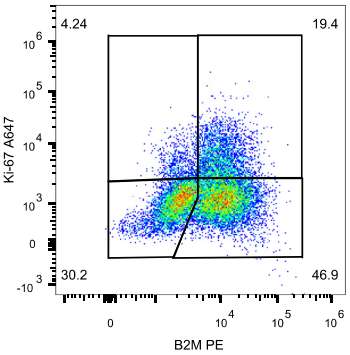

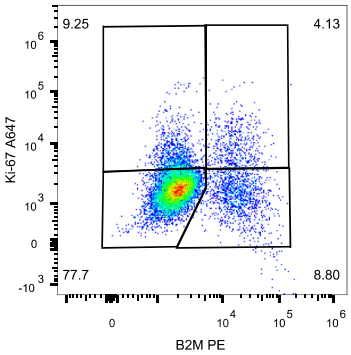

Day 15#

Day 22

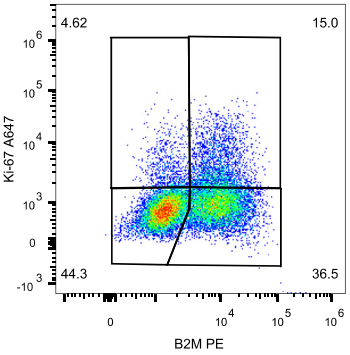

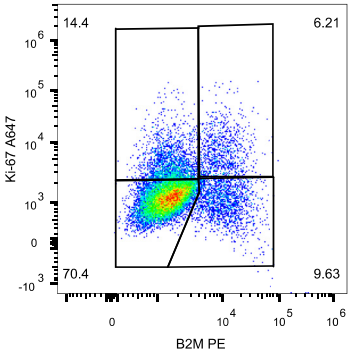

Day 22#

Day 29

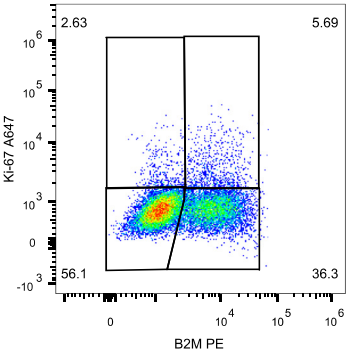

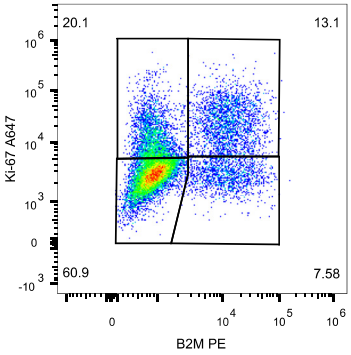

Day 29#

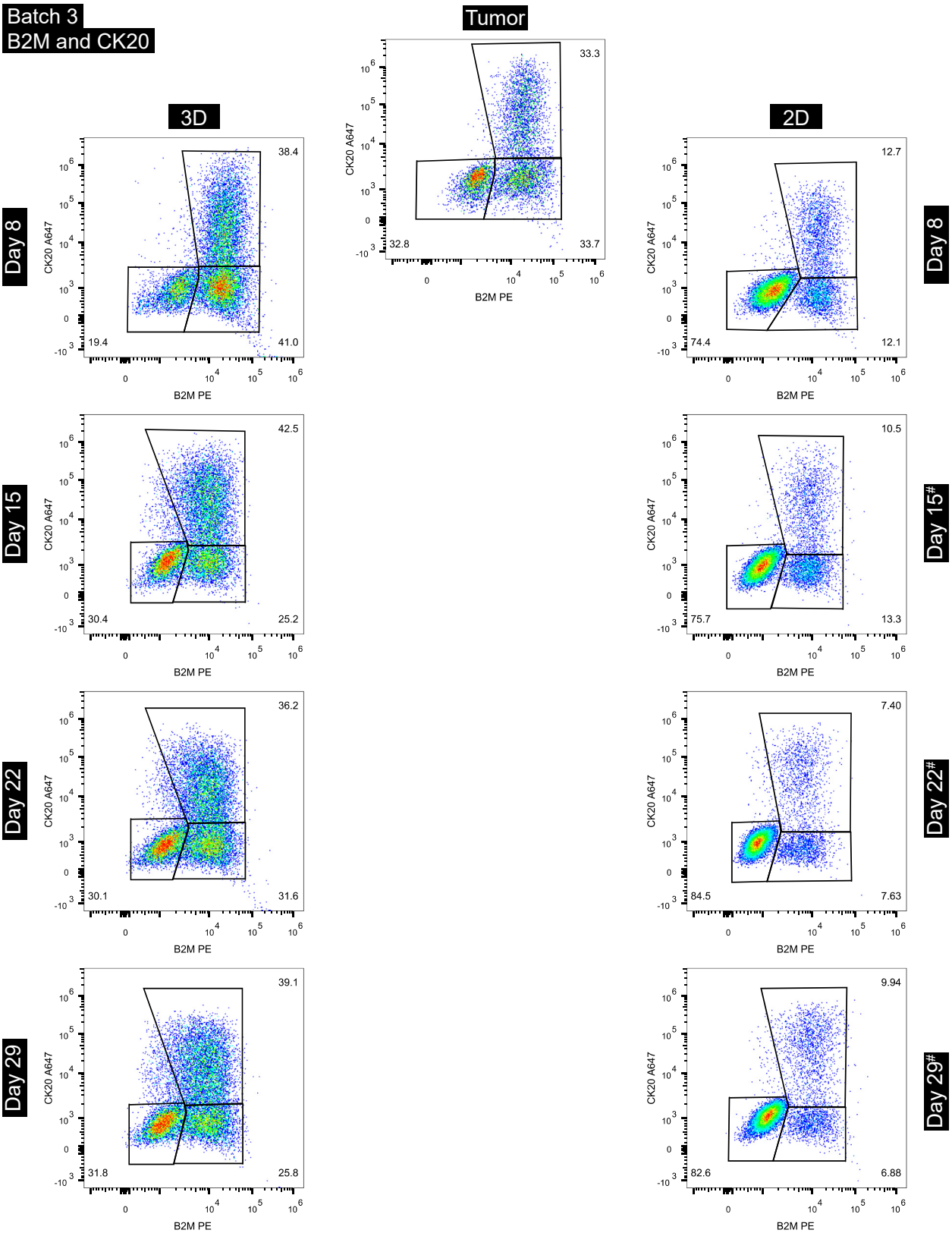
Batch 3
B2M and CK20
Tumor
3D
2D
Day 8
Day 15
Day 22
Day 29
Day 8
Day 15#
Day 22#
Day 29#
CK20 A647
B2M PE
33.3
32.8
33.7
38.4
19.4
41.0
12.7
74.4
12.1
42.5
30.4
25.2
10.5
75.7
13.3
36.2
30.1
31.6
7.40
84.5
7.63
39.1
31.8
25.8
9.94
82.6
6.88

Batch 3
B2M and Ki-67

Tumor

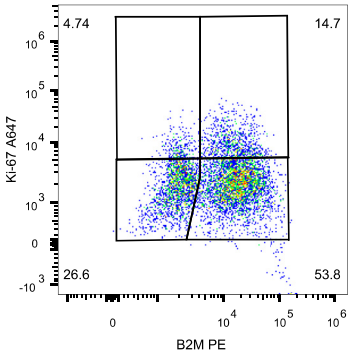

3D

2D

Day 8

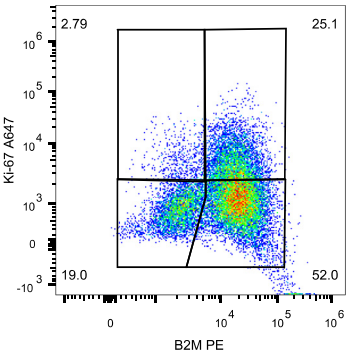

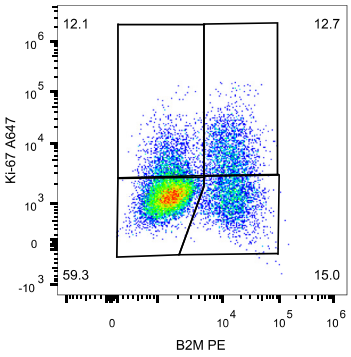

Day 8

Day 15

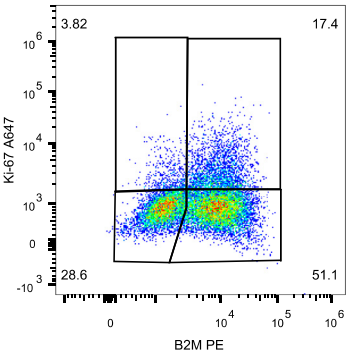

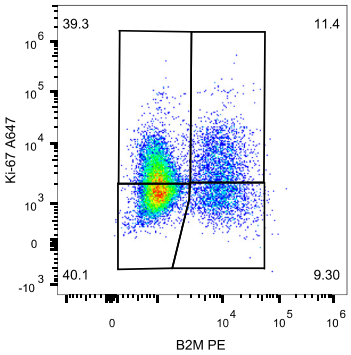

Day 15#

Day 22

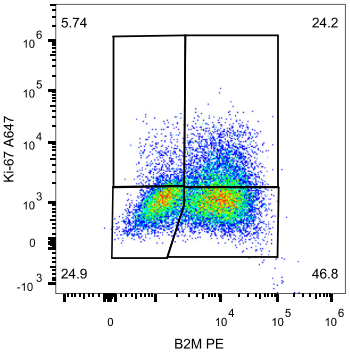

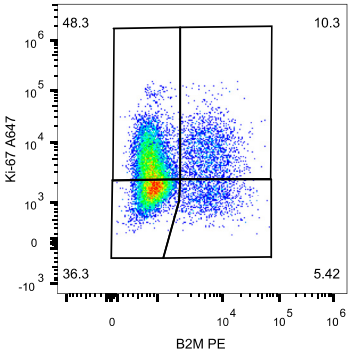

Day 22#

Day 29

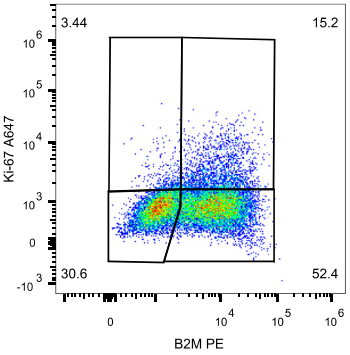

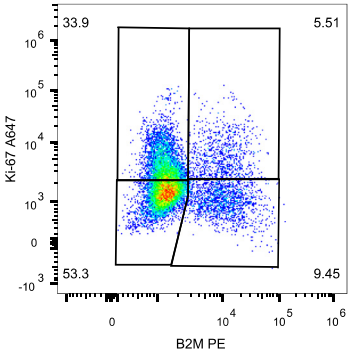

Day 29#

References

[1] Supek F, Bošnjak M, Škunca N and Šmuc T 2011 REVIGO summarizes and visualizes long lists of gene ontology terms *PloS one* **6** e21800